GEOLOGY | THE GEOLOGICAL SOCIETY OF AMERICA®

https://doi.org/10.1130/G46378.1

Manuscript received 22 May 2018
Revised manuscript received 20 May 2019
Manuscript accepted 22 May 2019

Mantle earthquakes in the Himalayan collision zone

Vera Schulte-Pelkum[1], Gaspar Monsalve[2], Anne F. Sheehan[1], Peter Shearer[3], Francis Wu[4], and Sudhir Rajaure[5]

[1]Cooperative Institute for Research in Environmental Sciences and Department of Geological Sciences, University of Colorado, Boulder, Colorado 80309, USA

[2]Facultad de Minas, Universidad Nacional de Colombia, Medellin, Colombia

[3]Institute for Geophysics and Planetary Physics, University of California, San Diego, La Jolla, California 92093, USA

[4]Department of Geology, Binghamton University, State University of New York, Binghamton, New York 13902, USA

[5]Department of Mines and Geology, Lainchaur, Kathmandu 44600, Nepal

ABSTRACT

Earthquakes are known to occur beneath southern Tibet at depths up to ~95 km. Whether these earthquakes occur within the lower crust thickened in the Himalayan collision or in the mantle is a matter of current debate. Here we compare vertical travel paths expressed as delay times between S and P arrivals for local events to delay times of P-to-S conversions from the Moho in receiver functions. The method removes most of the uncertainty introduced in standard analysis from using velocity models for depth location and migration. We show that deep seismicity in southern Tibet is unequivocally located beneath the Moho in the mantle. Deep seismicity in continental lithosphere occurs under normally ductile conditions and has therefore garnered interest in whether its occurrence is due to particularly cold temperatures or whether other factors are causing embrittlement of ductile material. Eclogitization in the subducting Indian crust has been proposed as a cause for the deep seismicity in this area. Our observation of seismicity in the mantle, falling below rather than within the crustal layer with proposed eclogitization, requires revisiting this concept and favors other embrittlement mechanisms that operate within mantle material.

INTRODUCTION

The Himalaya-Tibet continental collision zone has featured prominently in a debate on whether strength in the lithosphere resides in two layers in the brittle crust and uppermost mantle separated by a weak lower crust, or in a single layer largely limited to the crust (Chen et al., 1981, 2012; Chen and Molnar, 1983; Zhu and Helmberger, 1996; Henry et al., 1997; Cattin and Avouac, 2000; Jackson, 2002; Chen and Yang, 2004; Beaumont et al., 2004; Monsalve et al., 2006; de la Torre et al., 2007; Bendick and Flesch, 2007; Liang et al., 2008; Priestley et al., 2008; Craig et al., 2012). The distribution of seismicity with depth in strained regions serves as a proxy for the lithospheric strength profile because the occurrence of earthquakes implies sufficient strength to sustain brittle failure, due to either cold conditions (e.g., Chen and Molnar, 1983; Sloan and Jackson, 2012; Blanchette et al., 2018) or local embrittlement processes (e.g., Incel et al., 2017, 2019; Prieto et al., 2017). The task is therefore to map where exactly local earthquakes occur with respect to layers within the crustal and uppermost mantle column. A difficulty is posed by uncertainty in estimated depths for both local seismicity and the Moho. Crustal earthquake depths are more difficult to constrain than their epicenters because the stations used to locate them are on the surface and there is a strong tradeoff between location depth and P and S velocity structure above the events.

Intralithospheric interfaces such as the Moho can be seen with teleseismic converted waves (receiver functions), but determining their depth suffers from the same tradeoff with velocity structure above the interface as in estimating earthquake depths. Comparing hypocentral depths with structural depths is hampered by the uncertainties in both parameters. The comparison is accurate only if the same velocity models are used for depth determination for both data sets. More typically, results are compared between different studies, and a lack of consistency between the velocity models used exacerbates the uncertainties. We propose a simple workaround to the depth determination uncertainty by comparing seismicity and structure directly as delay times between shear and compressional waves ("S minus P", or S-P), rather than converting both to depth first.

DATA AND METHODS

We used data from the CE 2001–2003 HIMNT (Himalayan Nepal Tibet) seismic broadband experiment (Fig. 1). Of the seismicity located using the network (Monsalve et al., 2006), deep events are seen in Nepal just south of the Lesser Himalaya (Fig. 1, cluster C) and under Tibet (Fig. 1, clusters A and B). Figure 2B shows the same set of events on a previous structural depth profile from receiver functions on a line crossing the collision zone in a N18°E orientation perpendicular to the local range strike (Schulte-Pelkum et al., 2005). The Moho is visible as a contrast in isotropic velocity, and the Main Himalayan thrust as a contrast in anisotropy (Fig. 2B; Schulte-Pelkum et al., 2005). Even in this best-case scenario, with relocations and structural imaging done with the same stations and the same velocity models, the deep seismicity appears diffuse in depth and is difficult to clearly assign to crust or mantle.

Local earthquake depths are usually calculated from the travel-time difference between P and S arrivals from the event at each station. In receiver function studies, delays between teleseismic P and converted S are used to determine depths to interfaces under the station. In both cases, the S-P delay time is mapped to depth by assuming P and S velocity models between the event or converting interface and the station. Teleseismic arrivals and local events close to the station have similar steep incidence angles (Fig. 3C). Direct comparison of such S-P delay times between the two data sets therefore avoids the introduction of bias from using velocity models for depth migration and from unaccounted-for lateral variations, because the ray paths sample similar volumes. The two comparison data sets are constructed as follows.

Local Seismicity

For the local seismicity used in the S-P delay comparison, we used a previously relocated and published local event set of ~500 earthquakes (Monsalve et al., 2006; Fig. 1), each located with at least 10 P and S arrivals picked with the HIMNT network; pick statistics are shown

CITATION: Schulte-Pelkum, V., et al., 2019, Mantle earthquakes in the Himalayan collision zone: Geology, https://doi.org/10.1130/G46378.1

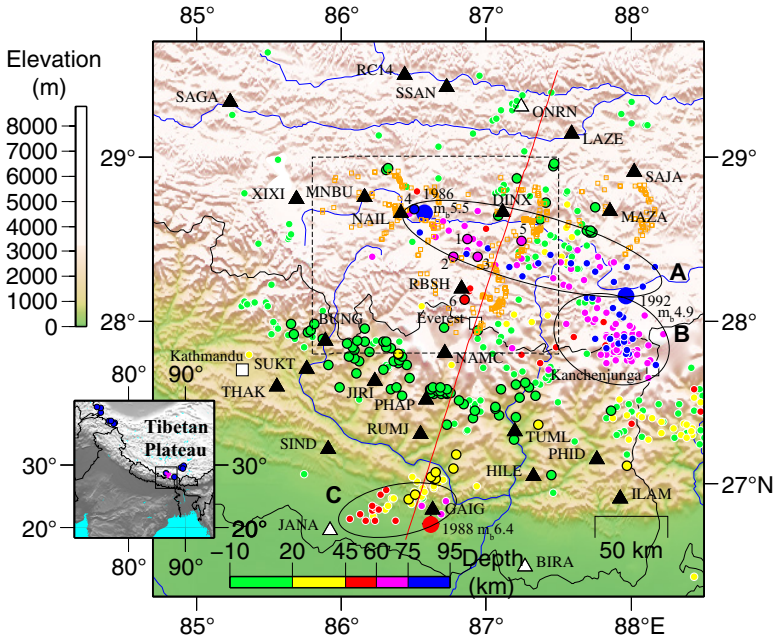

Figure 1. Map of study area, Himalaya-Tibet collision zone. Inset map shows regional geographical context, with gray shading showing topography for orientation. Blue circles in inset are 12 events from the compilation of Chen and Yang (2004) with depths of 80 km or more. Magenta open circles in inset map are our deep events 1–6 (Table DR1 [see footnote 1]). In large map, background color is elevation shaded by topography. Small circles are best-relocated local seismicity from 2001 to 2003 (Monsalve et al., 2006, 2008, 2009). Large circles are the three deep events from the compilation of Chen and Yang (2004, their events T8, T9, and T12; displayed here with event year and body wave magnitude) that fall within the map area. Events are color coded by depth below sea level. Small circles have thin white outline for events in the initial catalog (Monsalve et al., 2009; white circles in Fig. 2B) and thicker black outline for events used in delay-time analysis after selection for station distance, location error, and pick uncertainty (blue circles in Fig. 2B). Black triangles are HIMNT (Himalayan Nepal Tibet) stations used in this study. Red line marks the profile shown in Figures 2 and 3. White squares show locations of Kathmandu, Mount Everest, and Kanchenjunga. Black labeled ellipses roughly outline clusters of deep seismicity A–C discussed in the text; while the three larger events from Chen and Yang (2004) are located near them, the clusters' distribution in space, time, and magnitude do not fit aftershock characteristics (see the Data Repository). Dashed rectangle shows map area of Figure 4A, and pale orange squares show receiver function piercing points at 70 km depth for stations in Figure 4.

in Figure DR1 in the GSA Data Repository[1]. For each event in this catalog located within the network footprint, we selected stations with P and S picks at epicentral distances of <35 km to sample a near-station volume. For these event-station pairs, we calculated the time difference between S and P arrival pick times (S-P) and its uncertainty. The S-P pick uncertainty was calculated by propagating the original uncertainty in the P and S arrival picks. Pick uncertainty and location error have long-tailed distributions, and we chose their half-amplitude widths of ~0.2 s (S-P uncertainty) and 1 km (location error) as cutoff values (Fig. DR2), leaving 136 S-P differential arrival times from 98 events (black outlines in Fig. 1; blue events in Figs. 2B and 2C).

Structure from Receiver Functions

We used a previously published teleseismic Ps receiver function set from the HIMNT network (Schulte-Pelkum et al., 2005) to determine S-P times for the comparison to local seismicity. We additionally processed receiver functions to obtain a new higher-frequency set (Fig. 4) using automated event and receiver function quality-control criteria detailed by Schulte-Pelkum and Mahan (2014). Arrival times for the Moho conversion were picked from the original receiver function set for each station after corrections for slowness, with errors based on the width of the arrival and azimuthal variations seen at the station (Fig. 2C). A comparison with the second higher-frequency receiver function set shows close agreement in picked Moho times (examples in Fig. 4B). A group of stations in southern Tibet shows a positive amplitude arrival preceding the Moho peak (Fig. 4B), which marks the top of a layer with elevated lower-crustal velocities seen previously under this as well as other networks along the Himalaya (Yuan et al., 1997; Kind et al., 2002; Wittlinger et al., 2009; Schulte-Pelkum et al., 2005; Nábělek et al., 2009; Zhang et al., 2014). As in these studies, we picked the later arrival as the Moho at these stations because the resulting Moho is contiguous with that determined at neighboring stations. We also picked Main Himalayan thrust arrival times on the peak amplitude of the first azimuthal harmonic at each station (Schulte-Pelkum and Mahan, 2014).

Distance Correction

The events selected as above as well as the teleseismic receiver functions have steep ray paths under the stations and therefore sample similar structure. The S-P delay time is a function of the incidence angle. We applied a moveout correction to vertical incidence to the receiver function waveforms' time axis prior to picking the interface S-P times (Schulte-Pelkum et al., 2005), and applied a correction to the local event S-P time to mimic vertical incidence. The correction requires assumption of average crustal velocities between the event or interface in question and the station:

$$\Delta t_z = \sqrt{\Delta t^2 - d^2\left(\frac{1}{V_s} - \frac{1}{V_p}\right)^2}, \qquad (1)$$

(where Δt_z is the vertical time difference, Δt is the measured time difference, d is the epicentral distance, and Vp and Vs are the P and S wave speeds, respectively); so our S-P time comparison is not completely velocity free. However, Figure 3 demonstrates that the error introduced by a possible bias in velocity model is of second order because of the small epicentral distances involved, whereas a velocity model bias leads to a first-order error in depth determination.

After correcting all data to vertical incidence, we plotted the vertical S-P delay times from local seismicity and from teleseismic receiver functions on the same range-perpendicular profile (Fig. 2C). The profile is the same as the distance-depth profile in Figure 2B, but the vertical axis is now S-P delay time instead of depth. This representation introduces a distortion of the depth scale but minimizes the effect of the unknown velocity model (Fig. 3) and shows the relative depth relationship between the Moho and earthquake hypocenters. To test for any influence of lateral variations in Moho depth, we compare individual deep events to nearby receiver-function Moho piercing points in Figure 4.

RESULTS AND DISCUSSION

Potential mantle seismicity in the original set of ~500 events (Fig. 1, dots with black or white outlines) can be roughly grouped into three clusters (Fig. 1). Cluster B, just northwest of Kanchenjunga, falls outside our analysis set because of the lack of nearby stations. Deep events in cluster C near the CE 1988 near-Moho Udayapur earthquake (46–50 km estimated depths; summary in Ghimire and Kasahara, 2007) coincide with downtimes at HIMNT station GAIG or exceed the location or pick error criteria. Five events in cluster A (Fig. 1, dots with black outlines) pass our distance and uncertainty criteria, and all of them plot below the Moho in the S-P profile (Fig. 2C, between 0 and 50 km distance on the profile). These best-constrained events

[1]GSA Data Repository item 2019283, supplementary information (text, Figures DR1–DR4, and Table DR1), is available online at http://www.geosociety.org/datarepository/2019/, or on request from editing@geosociety.org.

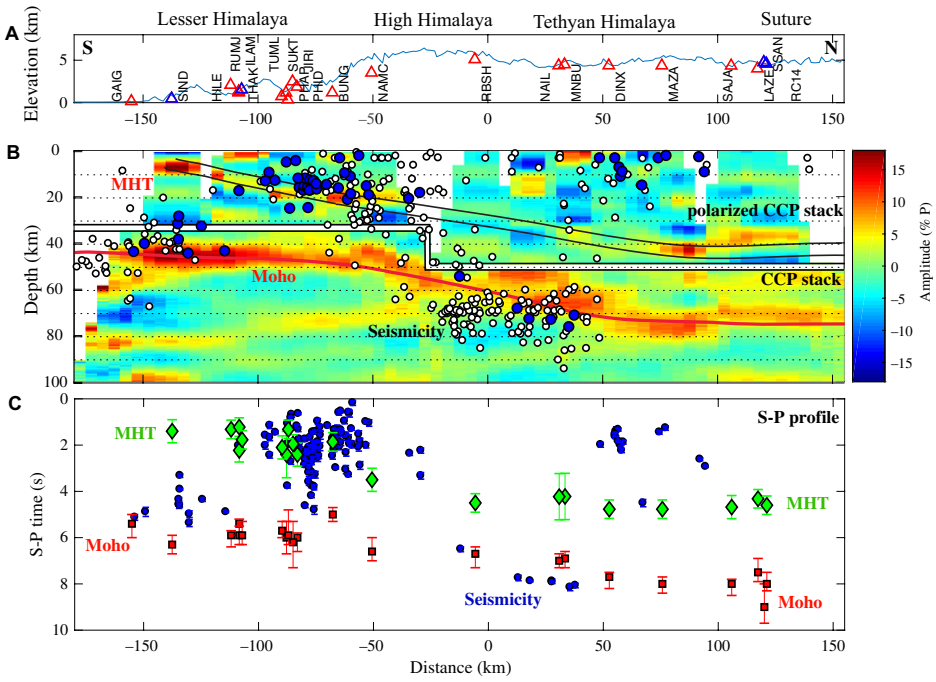

Figure 2. Depth profile along red line in Figure 1. A: Elevation profile. Triangles show HIMNT (Himalayan Nepal Tibet) seismic station locations. Red stations have event picks in the initial catalog, as well as Moho picks; blue stations have Moho picks only. B: Depth profile (depth relative to sea level). Above horizontal black-and-white breaks, background color shows polarized common-point-conversion (CCP) stack from receiver functions (Schulte-Pelkum et al., 2005); high amplitudes (red) are interpreted as the shear zone associated with the Main Himalayan thrust (MHT; marked approximately with black lines). Below black-and-white breaks, background color shows standard unpolarized CCP stack, with Moho traced in red. Seismicity in the initial catalog is shown as white circles. Blue circles are subset of events used in the S-to-P delay (S-P) profile after selection for station-event distance, location error, and pick error. C: Same profile as in B, but as function of S-P time instead of depth (see Fig. 3C). Red squares with error bars mark Moho pick times from receiver functions, plotted under each station. Red error bars are Moho pick uncertainties estimated from pulse width and azimuthal variation at each station. Green diamonds with error bars mark Main Himalayan thrust picks, with error bars representing uncertainty of arrival based on pulse width and variation of the peak time with backazimuth at each station. Blue circles with error bars are S-P pick times for blue events in B, plotted under each event epicenter (one event may have picks from several stations). Error bars on picks are uncertainties propagated from P and S pick uncertainties. The Monsalve et al. (2006) Tibet model is used for distance correction. Numbers 1–6 refer to events shown in Figure 4 and discussed in the text. Elevation correction is not applied because it only amounts to 0.1 s delay time per 1 km of elevation difference, and nearby stations and events are compared.

are not the deepest in the depth profile (Fig. 2B). An additional event just south of station RBSH plots within RBSH's Moho error bar on the S-P profile (Fig. 2C, near –10 km profile distance). The magnitudes of these six deep events range from M_L 2.4 to 2.9.

The larger error bar on the Moho time picked at station RBSH is due to azimuthal variations of the Moho pick in the receiver functions from that station. To exclude the influence of lateral variations in Moho depths or in velocities along ray paths, we compared deep-event S-P times to those from receiver functions with the closest piercing points. Figure 4A shows the map locations of the five sub-Moho and one near-Moho events in Figure 2C, as well as receiver function piercing points at 75 km depth for nearby stations. Figure 4B compares the S-P delay times of those events to receiver functions from nearby piercing points (larger dots in Fig. 4A). Receiver function stacks for those piercing points are shown for the same frequency band as used in the cross section in Figure 2B as well as for a higher-frequency band to obtain sharper Moho resolution. The shallower event south of RBSH (event 6) is below even shallower Moho picks for nearby piercing points. The considerable difference in Moho pick times between receiver functions from southern compared to northern back-azimuths at RBSH may represent actual Moho topography, but may also be due to lateral variations in velocity structure above the Moho.

The six deep events' delay times are 0.3–1.1 s larger than the Moho delay times (Fig. 4B). Using uppermost mantle velocities from the standard AK135 model (Kennett et al., 1995) as well as those for Tibet from Monsalve et al. (2006), this delay time range corresponds to event depths of 3–11 km below the Moho. None of the deep events in southern Tibet that pass the error and distance criteria plot above the Moho. In an S-P profile with more events including those with larger location errors and pick uncertainties (Fig. DR3), only one event plots above the error bar of the Moho in southern Tibet despite more scatter overall.

Shallower seismicity is concentrated in the southern Tibetan upper crust, with one event just above the Main Himalayan thrust (Fig. 2C, profile distances 0–150 km). No events are seen in the Indian crust (below the Main Himalayan thrust and above the Moho) under southern Tibet,

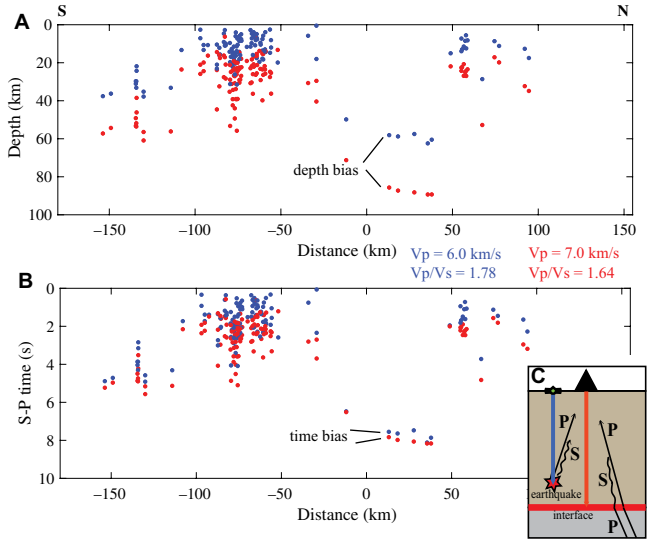

Figure 3. A: Earthquake depth bias introduced by the velocity model, shown on the same profile as in Figure 2. Blue dots are S-to-P delay (S-P) picks migrated to depth using the velocity model shown in blue text (middle left). Red dots are the same picks but migrated with the red velocity model (middle right). Lower Vp and higher Vp/Vs decrease migrated depth; the models were chosen to show the range of depths when using velocities from the Tibet model of (Monsalve et al., 2008). B: Same as in A, but with S-P time instead of depth. Blue and red dots are S-P picks corrected to vertical incidence using correspondingly colored model as for A. Note reduction in bias from using different velocity models compared to depth migration. Deep events show less change in S-P correction between models because of steeper ray paths. C: Cartoon illustrating method. Target is depth of local earthquake (blue line) relative to Moho depth (red line). Local seismicity (red star) close to station (triangle) has P and S ray paths with comparable steepness to teleseismic receiver function arrivals (right).

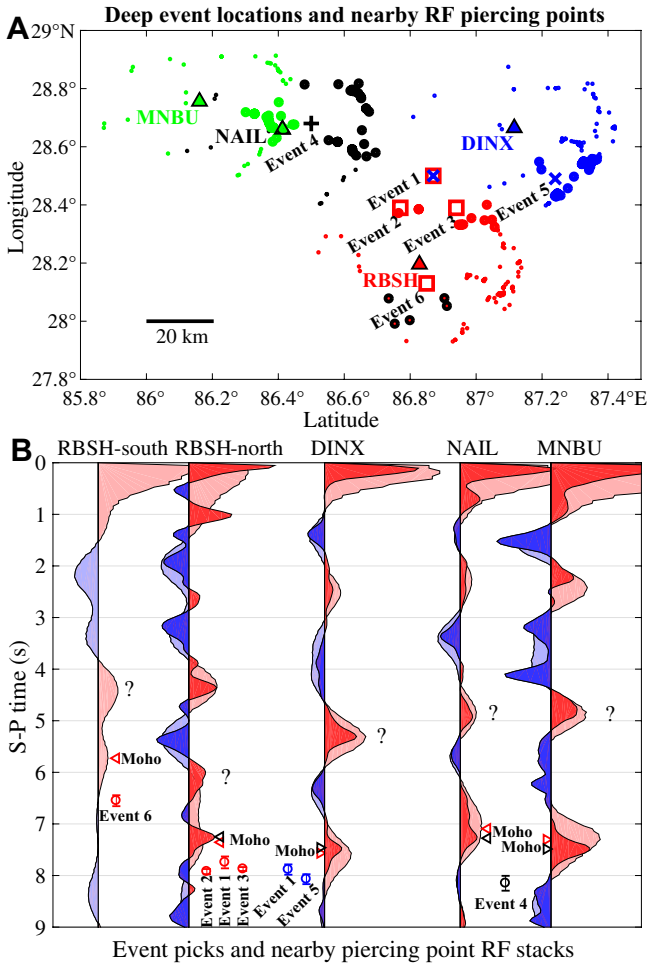

Figure 4. A: Map of HIMNT (Himalayan Nepal Tibet) seismic stations (triangles), receiver function (RF) piercing points at 75 km depth (small and large dots, with small dots showing all piercing points and large dots those for subsets of receiver functions at each station that were selected for proximity to events 1–6), and deep events (squares for events with selected S-P picks at RBSH; cross at NAIL; × at DINX) in dashed rectangle shown in Figure 1, encompassing all six near-Moho events and receiver function picks at profile distances –20 to 50 km as shown in Figure 2C. Receiver function piercing points are color coded to correspond to each station. Event symbols are also color coded to show which station has an S-to-P delay (S-P) pick fulfilling distance and error criteria (event 1 has picks at two stations). Moho picks and errors in Figure 2C are based on receiver functions from all piercing points (small dots). B: Radial component receiver function stacks using receiver functions with nearby piercing points (large dots in A) displayed next to closest deep events. Time is S-P time and is corrected to vertical incidence. Red amplitudes are positive polarity; blue, negative. Lighter-colored (semitransparent) receiver functions are calculated with Gaussian filter factor of 3 (Ligorría and Ammon, 1999); darker (more opaque), using higher-frequency Gaussian filter factor 7. RBSH-south stack is for piercing points in red with black outline in A; for this stack with smallest number of receiver functions in the figure, none of the high-frequency traces passed deconvolution criteria due to higher noise in this band. Stations are sorted roughly south (left) to north (right) and by vicinity to events close to each other. Triangles show Moho peak in receiver functions for lower (red) and higher (black) frequency band. Question marks are arrivals that may stem from top of high-velocity lower crustal layer identified in other studies cited in text.

from ~ –50 km profile distance to the north. This bimodal depth distribution in seismicity and the concentration of deep seismicity in cluster A persists from the 2001–2003 recording period of the HIMNT network (Monsalve et al., 2006; Huang et al., 2009) through the 2003–2005 period of the HI-CLIMB (Himalayan-Tibetan Continental Lithosphere during Mountain Building) network (Liang et al., 2008; Carpenter, 2010), which covered a footprint including that of HIMNT. Combining this catalog for the 2001–2005 time span with our placement of the deep seismicity below the Moho, we conclude that the seismicity in the Tibetan portion of the profile (north of the High Himalaya) shows a seismogenic upper (Asian) crust, an aseismic middle and lower (Indian) crust, and a seismogenic mantle.

In Nepal, seismicity is focused near the Main Himalayan thrust downdip from the locked portion (profile distances –120 to –20 km), and is distributed through all crustal levels south of the Lesser Himalaya (distances –180 to –120 km). Mantle seismicity in this area is seen in other studies (Monsalve et al., 2006; Huang et al., 2009) and is also suggested by our S-P profile when including events with larger location and pick errors (Fig. DR3). In contrast to the bimodal depth distribution north of the High Himalaya, the Indian plate therefore appears as a single seismogenic layer in this region before it begins its descent under the Himalaya.

Continental lower crust and mantle should normally deform in the ductile regime, and the presence of seismicity at these depths requires either cold material (<~600 °C; Chen and Molnar, 1983; Sloan and Jackson, 2012) or mechanisms that allow brittle failure under higher-than-normal temperature and pressure conditions (Thielmann et al., 2015; Incel et al., 2017, 2019). Eclogitization of a metastable subducting Indian continental lower crust in the presence of water has been proposed as a source for the deep seismicity under Tibet (Lund et al., 2004; Jackson et al., 2004; Jamtveit et al., 2018). While the presence of higher-than-average velocities in the Indian lower crust under Tibet supports eclogitization (Schulte-Pelkum et al., 2005; Monsalve et al., 2006, 2008; Hetényi et al., 2007; Huang et al., 2009), our observation that the seismicity is in the mantle rather than the lower crust in this location contradicts the interpretation that eclogitization triggers deep crustal seismicity.

While seismicity in the mantle has been interpreted as requiring temperatures <600 °C (e.g., Jackson et al., 2008), there are embrittlement mechanisms in the mantle under ductile conditions that do not require cold temperatures, such as dehydration embrittlement, thermal runaway shear, and grain-size reduction (e.g., Kelemen and Hirth, 2007; Thielmann et al., 2015; Incel et al., 2017). Continental mantle earthquakes have been observed in regions of high temperatures (e.g., in southern California, USA; Inbal et al., 2016) and with rupture characteristics supporting such mechanisms (e.g., for the deep mantle seismicity under the Wyoming province, USA; Prieto et al., 2017). The laterally clustered nature of the deep seismicity in southern Tibet (Fig. 1; Monsalve et al., 2006, 2009; Huang et al., 2009; Carpenter, 2010) may point toward such mechanisms operating locally.

ACKNOWLEDGMENTS

We acknowledge field efforts by R. Bilham and the HIMNT field teams, and discussions with P. Molnar, T. Stern, and K. Mahan. Comments by the editor, two anonymous reviewers, Hélène Lyon-Caen, Alexander Blanchette, and Simon Klemperer helped improve the manuscript significantly. This research was supported by U.S. National Science Foundation grants EAR-0310372, EAR-0538259, EAR-1246287, and EAR-1645009.

REFERENCES CITED

Beaumont, C., Jamieson, R.A., Nguyen, M.H., and Medvedev, S., 2004, Crustal channel flows: 1. Numerical models with applications to the tectonics of the Himalayan-Tibetan orogen: Journal of Geophysical Research, v. 109, B06406, https://doi.org/10.1029/2003JB002809.

Bendick, R., and Flesch, L., 2007, Reconciling lithospheric deformation and lower crustal flow beneath central Tibet: Geology, v. 35, p. 895–898, https://doi.org/10.1130/G23714A.1.

Blanchette, A.R., Klemperer, S.L., Mooney, W.D., and Zahran, H.M., 2018, Two-stage Red Sea rifting inferred from mantle earthquakes in Neoproterozoic lithosphere: Earth and Planetary Science Letters, v. 497, p. 92–101, https://doi.org/10.1016/j.epsl.2018.05.048.

Carpenter, N.S., 2010, South-central Tibetan seismicity recorded by HiCLIMB seismic array [M.S. thesis]: Corvallis, Oregon State University, 228 p.

Cattin, J., and Avouac, J.-P., 2000, Mountain building and the seismic cycle in the Himalaya of Nepal: Journal of Geophysical Research, v. 105,

p. 13,389–13,407, https://doi.org/10.1029/2000JB900032.

Chen, W.-P., and Molnar, P., 1983, Focal depths of intracontinental and intraplate earthquakes and their implications for the thermal and mechanical properties of the lithosphere: Journal of Geophysical Research, v. 88, p. 4183–4214, https://doi.org/10.1029/JB088iB05p04183.

Chen, W.-P., and Yang, Z., 2004, Earthquakes beneath the Himalayas and Tibet: Evidence for strong lithospheric mantle: Science, v. 304, p. 1949–1952, https://doi.org/10.1126/science.1097324.

Chen, W.-P., Nábělek, J.L., Fitch, T.J., and Molnar, P., 1981, An intermediate depth earthquake beneath Tibet: Source characteristics of the event of September 14, 1976: Journal of Geophysical Research, v. 86, p. 2863–2876, https://doi.org/10.1029/JB086iB04p02863.

Chen, W.-P., Hung, S.-H., Tseng, T.-L., Brudzinski, M., Yang, Z., and Nowack, R.L., 2012, Rheology of the continental lithosphere: Progress and new perspectives: Gondwana Research, v. 21, p. 4–18, https://doi.org/10.1016/j.gr.2011.07.013.

Craig, T.J., Copley, A., and Jackson, J., 2012, Thermal and tectonic consequences of India underthrusting Tibet: Earth and Planetary Science Letters, v. 353–354, p. 231–239, https://doi.org/10.1016/j.epsl.2012.07.010.

de la Torre, T.L., Monsalve, G., Sheehan, A.F., Sapkota, S., and Wu, F., 2007, Earthquake processes of the Himalayan collision zone in eastern Nepal and the southern Tibetan Plateau: Geophysical Journal International, v. 171, p. 718–738, https://doi.org/10.1111/j.1365-246X.2007.03537.x.

Ghimire, S., and Kasahara, M., 2007, Source process of the Ms = 6.6, Udayapur earthquake of the Nepal-India border and its tectonic implication: Journal of Asian Earth Sciences, v. 31, p. 128–138, https://doi.org/10.1016/j.jseaes.2007.04.007.

Henry, P., Le Pichon, X., and Goffé, B., 1997, Kinematic, thermal and petrological model of the Himalayas: Constraints related to metamorphism within the underthrust Indian crust and topographic elevation: Tectonophysics, v. 273, p. 31–56, https://doi.org/10.1016/S0040-1951(96)00287-9.

Hetényi, G., Cattin, R., Brunet, F., Bollinger, L., Vergne, J., Nábe⊠lek, J., and Diament, M., 2007, Density distribution of the India plate beneath the Tibetan plateau: Geophysical and petrological constraints on the kinetics of lower-crustal eclogitization: Earth and Planetary Science Letters, v. 264, p. 226–244, https://doi.org/10.1016/j.epsl.2007.09.036.

Huang, G.-C., Wu, F.T., Roecker, S.W., and Sheehan, A.F., 2009, Lithospheric structure of the central Himalaya from 3-D tomographic imaging: Tectonophysics, v. 475, p. 524–543, https://doi.org/10.1016/j.tecto.2009.06.023.

Inbal, A., Ampuero, J.P., and Clayton, R.W., 2016, Localized seismic deformation in the upper mantle revealed by dense seismic arrays: Science, v. 354, p. 88–92, https://doi.org/10.1126/science.aaf1370.

Incel, S., Hilairet, N., Labrousse, L., John, T., Deldicque, D., Ferrand, T., Wang, Y., Renner, J., Morales, L., and Schubnel, A., 2017, Laboratory earthquakes triggered during eclogitization of lawsonite-bearing blueschist: Earth and Planetary Science Letters, v. 459, p. 320–331, https://doi.org/10.1016/j.epsl.2016.11.047.

Incel, S., et al., 2019, Reaction-induced embrittlement of the lower continental crust: Geology, v. 47, p. 235–238, https://doi.org/10.1130/G45527.1.

Jackson, J., 2002, Strength of the continental lithosphere: Time to abandon the jelly sandwich?: GSA Today, v. 12, no. 9, p. 4–9, https://doi.org/10.1130/1052-5173(2002)012<0004:SOTCLT>2.0.CO;2.

Jackson, J., McKenzie, D., Priestley, K., and Emmerson, B., 2008, New views on the structure and rheology of the lithosphere: Journal of the Geological Society [London], v. 165, p. 453–465, https://doi.org/10.1144/0016-76492007-109.

Jackson, J.A., Austrheim, H., McKenzie, D., and Priestley, K., 2004, Metastability, mechanical strength, and the support of mountain belts: Geology, v. 32, p. 625–628, https://doi.org/10.1130/G20397.1.

Jamtveit, B., Ben-Zion, Y., Renard, F., and Austrheim, H., 2018, Earthquake-induced transformation of the lower crust: Nature, v. 556, p. 487–491, https://doi.org/10.1038/s41586-018-0045-y.

Kelemen, P.B., and Hirth, J., 2007, A periodic shear-heating mechanism for intermediate-depth earthquakes in the mantle: Nature, v. 446, p. 787–790, https://doi.org/10.1038/nature05717.

Kennett, B.L.N., Engdahl, E.R., and Buland, R., 1995, Constraints on seismic velocities in the earth from travel times: Geophysical Journal International, v. 122, p. 108–124.

Kind, R., et al., 2002, Seismic images of the crust and upper mantle beneath Tibet: Evidence for Eurasian plate subduction: Science, v. 298, p. 1219–1221, https://doi.org/10.1126/science.1078115.

Liang, X., Zho, S., Chen, Y.J., Jin, G., Xiao, L., Liu, P., Fu, Y., Tang, X., Lou, X., and Ning, J., 2008, Earthquake distribution in southern Tibet and its tectonic implications: Journal of Geophysical Research, v. 113, B12409, https://doi.org/10.1029/2007JB005101.

Ligorría, J.P., and Ammon, C.J., 1999, Iterative deconvolution and receiver-function estimation: Bulletin of the Seismological Society of America, v. 89, p. 1395–1400.

Lund, M.G., Austrheim, H., and Erambert, M., 2004, Earthquakes in the deep continental crust—Insights from studies on exhumed high-pressure rocks: Geophysical Journal International, v. 158, p. 569–576, https://doi.org/10.1111/j.1365-246X.2004.02368.x.

Monsalve, G., Sheehan, A., Schulte-Pelkum, V., Rajaure, S., Pandey, M.R., and Wu, F., 2006, Seismicity and one-dimensional velocity structure of the Himalayan collision zone: Earthquakes in the crust and upper mantle: Journal of Geophysical Research, v. 111, B10301, https://doi.org/10.1029/2005JB004062.

Monsalve, G., Sheehan, A., Rowe, C., and Rajaure, S., 2008, Seismic structure of the crust and the upper mantle beneath the Himalayas: Evidence for eclogitization of lower crustal rocks in the Indian Plate: Journal of Geophysical Research, v. 113, B08315, https://doi.org/10.1029/2007JB005424.

Monsalve, G., McGovern, P., and Sheehan, A., 2009, Mantle fault zones beneath the Himalayan collision: Flexure of the continental lithosphere: Tectonophysics, v. 477, p. 66–76, https://doi.org/10.1016/j.tecto.2008.12.014.

Nábělek, J., Hetényi, G., Vergne, J., Sapkota, S., Kafle, B., Jiang, M., Su, H., Chen, J., Huang, B.-S., and the Hi-CLIMB Team, 2009, Underplating in the Himalaya-Tibet collision zone revealed by the Hi-CLIMB experiment: Science, v. 325, p. 1371–1374, https://doi.org/10.1126/science.1167719.

Priestley, K., Jackson, J., and McKenzie, D., 2008, Lithospheric structure and deep earthquakes beneath India, the Himalaya and southern Tibet: Geophysical Journal International, v. 172, p. 345–362, https://doi.org/10.1111/j.1365-246X.2007.03636.x.

Prieto, G.A., Froment, B., Yu, C., Poli, P., and Abercrombie, R., 2017, Earthquake rupture below the brittle-ductile transition in continental lithospheric mantle: Science Advances, v. 3, e1602642, https://doi.org/10.1126/sciadv.1602642.

Schulte-Pelkum, V., and Mahan, K.H., 2014, A method for mapping crustal deformation and anisotropy with receiver functions and first results from USArray: Earth and Planetary Science Letters, v. 402, p. 221–233, https://doi.org/10.1016/j.epsl.2014.01.050.

Schulte-Pelkum, V., Monsalve, G., Sheehan, A., Pandey, M.R., Sapkota, S., Bilham, R., and Wu, F., 2005, Imaging the Indian subcontinent beneath the Himalaya: Nature, v. 435, p. 1222–1225, https://doi.org/10.1038/nature03678.

Sloan, R.A., and Jackson, J.A., 2012, Upper-mantle earthquakes beneath the Arafura Sea and south Aru Trough: Implications for continental rheology: Journal of Geophysical Research, v. 177, B05402, https://doi.org/10.1029/2011JB008992.

Thielmann, M., Rozel, A., Kaus, B.J.P., and Ricard, Y., 2015, Intermediate-depth earthquake generation and shear zone formation caused by grain size reduction and shear heating: Geology, v. 43, p. 791–794, https://doi.org/10.1130/G36864.1.

Wittlinger, G., Farra, V., Hetényi, G., Vergne, J., and Nábělek, J., 2009, Seismic velocities in Southern Tibet lower crust: A receiver function approach for eclogite detection: Geophysical Journal International, v. 177, p. 1037–1049, https://doi.org/10.1111/j.1365-246X.2008.04084.x.

Yuan, X., Ni, J., Kind, R., Mechie, J., and Sandvol, E., 1997, Lithospheric and upper mantle structure of southern Tibet from a seismological passive source experiment: Journal of Geophysical Research, v. 102, p. 27,491–27,500, https://doi.org/10.1029/97JB02379.

Zhang, Z., Wang, Y., Houseman, G.A., Xu, T., Wu, Z., Yuan, X., Chen, Y., Tian, X., Bai, Z., and Teng, J., 2014, The Moho beneath western Tibet: Shear zones and eclogitization in the lower crust: Earth and Planetary Science Letters, v. 408, p. 370–377, https://doi.org/10.1016/j.epsl.2014.10.022.

Zhu, L., and Helmberger, D.V., 1996, Intermediate depth earthquakes beneath the India-Tibet collision zone: Geophysical Research Letters, v. 23, p. 435–438, https://doi.org/10.1029/96GL00385.

Printed in USA